Proceedings of the 9th International Conference on Civil Structural and Transportation Engineering (ICCSTE 2024)
Chestnut Conference Centre - University of Toronto, Toronto, Canada – June 13-15, 2024
Paper No. 169
DOI: 10.11159/iccste24.169

Bond Behavior of Ribbed Steel Bars or Seven-wire Strands in Lightweight Aggregate Concrete: A Numerical and Analytical Investigation

Zaher Alkurdi
Budapest University of Technology and Economics
Műegyetem rkp. 3, 1111, Budapest, Hungary
zaherkurdi@edu.bme.hu

Abstract **-** The diameter of the bar is a fundamental factor influencing bond behavior, and it continues to be a subject of interest due to conflicting opinions regarding its impact on bond behavior in pull-out tests. This study aimed to assess the impact of ribbed steel bar (B500B) and seven-wire strand (grade 1860) diameters on bond behavior, employing both numerical and analytical methods. Utilizing ATENA 3D software, finite element (FE) models were constructed, and a variety of formulae were applied for analytical computations. The FE models were validated by comparing them with existing experimental and analytical results. The materials employed included reinforcement bars with diameters ranging from 8 to 17.8 mm and lightweight aggregate concrete with a compressive strength of 41.65 MPa. The FE results revealed a slight decrease in bond strength with an increase in bar diameter. This decrease can be attributed to the larger contact area resulting from the increased bar diameter, which surpasses the effect of force and leads to a reduction in bond strength. Furthermore, the bond strength between the ribbed steel bar and concrete was approximately twice that of the seven-wire strand when embedded in concrete.

Keywords**:** pull-out test, bond, ATENA 3D software, lightweight aggregate concrete, seven-wire strand, interface element

1. Introduction

Concrete is a widely used material in construction, playing a vital role in the development of infrastructure in many countries [1]. In reinforced concrete structures, failure typically occurs due to a weakening of the bond between the materials. Composite action between concrete and embedded reinforcement is ensured by the bond developing on the interface during the hardening process of concrete. The pull-out test is commonly employed for measuring local bond strength and offering insights into the bond behavior between concrete and reinforcing bars [2]. The bond is characterized by the local bond stress–slip relationship influenced by various factors such as characteristics of the reinforcing unit (such as bar, multiwire strand, tendon), properties of the concrete, length, and diameter of the embedded bar, environmental exposure, and cyclic loading [3].

The bar diameter is still a factor of interest due to differing opinions on its effect on bond behavior during the pull-out test [4]. Certain studies have proposed a positive link between bar diameter and bond strength [5–7], while others have indicated a negative association [8–10], and still, some have found no significant correlation at all [11–13]. Yoo and Shin [14] investigated deformed steel rebar bond performance in ultra-high-strength concrete (12.7, 15.9, and 19.1 mm diameters). They observed a slight decrease in average bond strength with increasing bar diameter (Figure 1). This reduction in bond strength is linked to nonuniform bond stress distribution in high-strength concrete, influenced by the enhanced bearing capacity of concrete keys, contrasting with uniform distribution in normal strength concrete. Burdziński et al. [11] emphasized the crucial role of bar diameter in determining concrete block dimensions and bond behavior in the pull-out test. For bond lengths within five times the bar diameter, uniform distribution of bond stress on the lateral surface leads to similar maximum bond stress values across various diameters, influencing grouping by diameter. Tavares et al. [15] observed a direct correlation between ribbed steel bar diameter and bond strength, attributing the increased strength to a larger concrete contact area, enhanced sliding resistance, and elevated stress levels causing cracking at the peak load.

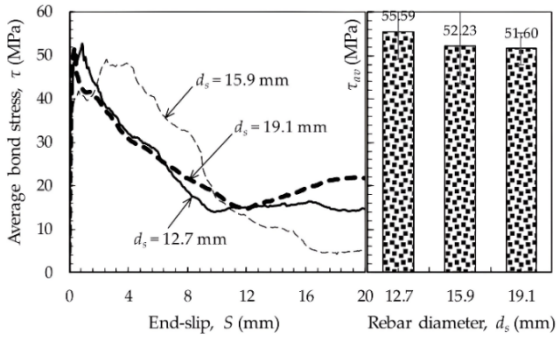

Figure 1: Effect of bar diameter on bond performance of ultra-high strength concrete according to Yoo and Shin [14].

The literature currently lacks sufficient experimental data regarding the bond characteristics of steel prestressing strands despite their extensive use in the prefabrication industry. Characterizing bond behavior in pre-tensioning anchorage involves distinguishing prestress transfer in the transmission length from anchoring the tendon tensile force during external loads in the flexural bond length [16]. In the transmission length, a scenario referred to as "push-in" unfolds, marked by longitudinal shortening and transverse expansion upon prestress release. Conversely, in the flexural bond length, the "pull-out" situation occurs, where tendons contract and pull due to increasing bending stress in the bending crack.

Lightweight concrete (LWC) has many benefits for reinforced concrete structures, such as reduced density leading to improved design efficiency, easier handling and transport, and lower design loads [17]. However, various attributes of LWC, such as the bond behavior of used reinforcing, have not been described thoroughly. Abed et al. [18] simulated pull-out tests using ATENA 3D software to compare the bond behavior of ribbed steel bars and seven-wire strands in LWC. Their conclusion aligns with Gulyás et al. [19] and fib Bulletin 51 [20], stating that seven-wire strands exhibit approximately 60% lower bond strength in concrete compared to ribbed steel bars. Kovács et al. [3] compared the bond behavior of steel bars in LWC with expanded clay aggregate to normal weight concrete using standard pull-out tests. Results indicated similar bond strength for both concretes, with higher standard deviation in pull-out tests compared to compression and splitting tensile strength tests. Additionally, the characteristic bond strength–slip curve shape and failure mode were similar for LWC and normal weight concrete.

Numerical modeling has made considerable progress in this area. Furthermore, numerical modeling is often implemented in design because experiments can be challenging, costly, and time-consuming [21]. In addition, model predictions closely align with experimental testing [22–25]. FE modeling of the interface between concrete and reinforcement is still not widely found in the literature. Current numerical models of concrete and steel reinforcement rarely consider bond, and analytical procedures consider bond in a simple way. There are typically two basic ways of modeling a bar or anchor being pulled out from concrete: the first involves a one-dimensional bar with a bond, while the second involves volume and three-dimensional (3D) interface elements [26]. To gain a more comprehensive comprehension of the bonding mechanism, the impact of various factors on the bond, and to provide a complete explanation of the failure mode, numerous researchers have employed finite element (FE) software [27–30] like ABAQUS [31], ANSYS [32], and ATENA [33]. Abed et al. [25] simulated pull-out tests using ATENA 3D software, defining a bond stress-slip curve based on experiments for the specific concrete and reinforcing bar materials. The numerical results closely matched the experimental data, capturing real behavior. Nardin et al. [34] simulated steel-concrete interface behavior with ANSYS and ABAQUS, focusing on 10 mm deformed bars and 30 MPa concrete. Their numerical study utilized non-linear material behavior for concrete and reinforcing bars, incorporating a model for their interaction. Results revealed that ABAQUS excelled in representing the ultimate load, while ANSYS captured the general behavior of the pre-peak branch more effectively.

Numerous researchers have highlighted the complexity and challenges associated with numerically modeling the bond, presenting a significant contact problem [34]. Ongoing debates within the literature surround the influence of bar diameter on bond behavior in pull-out tests. This study aims to enhance numerical modeling techniques, striving for improved accuracy

in FE models representing the concrete-reinforcement interface. The overarching goal is to unravel the intricacies of bond behavior between concrete and steel reinforcement, identifying crucial parameters and establishing interface element characteristics based on the Coulomb–Mohr criterion. As a result, the objective is to develop a comprehensive FE model capable of effectively simulating pull-out tests for various types and diameters of reinforcing bars.

2. Methodology

In this study, a combination of numerical modeling and analytical calculations was employed to enhance the understanding of bond behavior between reinforcement and concrete. The investigation covered diverse types of steel bars, such as ribbed steel bars and seven-wire strands, with diameters ranging from 8 mm to 17.8 mm. The analysis incorporated insights from a referenced experimental test [3] and a formula code [20]. ATENA [33], specifically designed for concrete, facilitated easier use due to reliable default values. This was accomplished by developing FE models for the pull-out test, which involves determining the interface parameters and proposing an empirical expression for the friction and cohesion coefficients. The research was focused on examining the influence of bar diameter on bond strength, utilizing FE models with different reinforcement diameters and conducting analytical calculations with multiple (fib MC2010 [12], Harajli et al. [35], AS 3600 [36], Orangun et al. [9], and Darwin et al. [37]).

2.1. Model of Contact (Interface) Elements

The 3D isoparametric gap element approach, implemented in ATENA 3D (referred to as the CCIsoGap element [33]), utilizes the Mohr-Coulomb friction law with an ellipsoidal tension cut-off. Figure 2 illustrates the general configuration of a quadrilateral element. This formulation employs quadrilateral or triangular plane elements on each contact surface, connected by unidirectional springs in all degrees of freedom. Interpolation techniques between the surface nodes' displacements determine relative displacements, which are then linked to traction forces (F_r and F_s) and the opening force (F_σ) through relevant constitutive relationships outlined in Equation 1. The matrix of coefficients includes K_{rr} and K_{ss}, corresponding to traction stiffness coefficients in the local directions r and s, respectively, while $K_{\sigma\sigma}$ represents the normal stiffness coefficient in the local direction w. The relative displacements (Δ_r, Δ_s, and Δ_ω) denote displacements between nodal pairs according to their respective directions. Contact elements within numerical models were employed to replicate the interplay between normal and tangential stresses on the compression side. This interaction was characterized by the initial Mohr-Coulomb surface, as expressed in Equation 2. For each stress component acting on the interface, trial stress was applied to the initial surface of the sliding opening interaction. Upon surpassing the transverse strength of the interface, the interaction surface transitioned to a residual failure surface, indicating dry friction. On the tension side, the strength curve conformed to an ellipsoidal shape until reaching the maximum value of tensile strength. After this threshold, a complete loss of the normal capacity of the interface ensued, resulting in the dislocation of the opposing surfaces. This methodology facilitated the longitudinal translation of the bar, inducing radial deformation, which, in turn, generated confining stresses through the interplay between shear and normal stresses at the bonded interface.

$$\begin{bmatrix} F_r \\ F_s \\ F_\sigma \end{bmatrix} = \begin{bmatrix} K_{rr} & 0 & 0 \\ 0 & K_{ss} & 0 \\ 0 & 0 & K_{\sigma\sigma} \end{bmatrix} . \begin{bmatrix} \Delta_r \\ \Delta_s \\ \Delta_\omega \end{bmatrix} \quad (1)$$

$$\tau = c + \sigma . \tan(\mu) \quad (2)$$

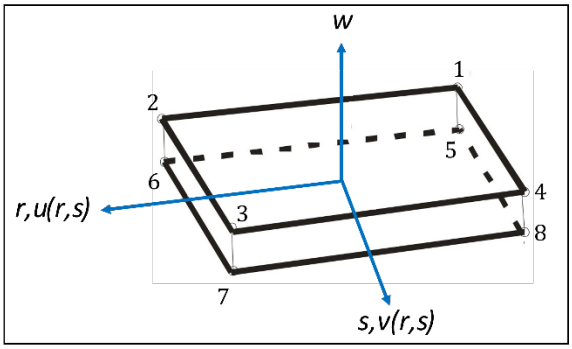

Figure 2: Interface CCIsoGap element [33].

2.2. Computational Modeling of Pull-out Test

The pull-out test was simulated using ATENA 3D software. The test was performed in accordance with the RILEM recommendation for steel reinforcement [38,39], as shown in Figure 3. A cubic specimen measuring 15 cm was prepared, wherein the reinforcement was embedded inside the cube. The embedment length was five times the diameter of the reinforcement. The simulations focused on two types of reinforcement: ribbed steel bars and seven-wire strands. To accomplish this, the parameters of the 3D interface material were determined based on a combination of previously reported experimental results for the ribbed steel bar specimen and the formula provided by fib Bulletin 51 [20] for the seven-wire strand specimen, represented by Equation 3.

$$\tau_{max,strand} = \sqrt{f'_c} \tag{3}$$

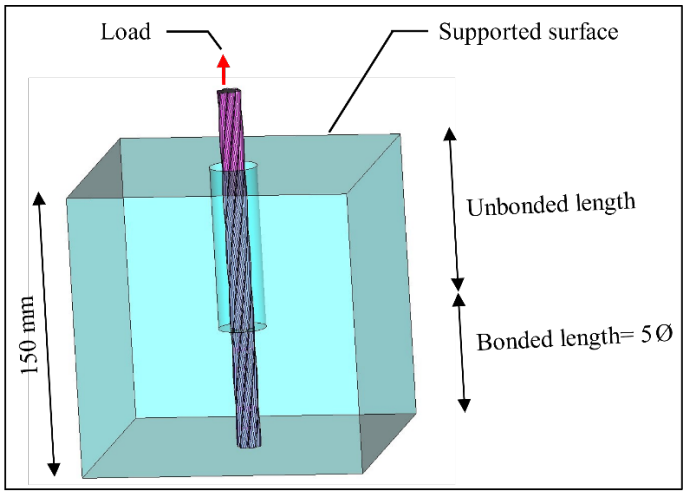

Figure 3: Schematic of the pull-out test specimen.

The specimen with a ribbed steel bar, detailed in the previous reference [3], had LWC with an average compressive strength of 41.65 MPa and an average tensile strength of 2.58 MPa. Additionally, the concrete exhibited an elastic modulus of 20.211 GPa and a density of 1744 kg/m^3. The chosen ribbed steel bar was of B500B type, with an 8 mm diameter, a cross-sectional area of 50.27 mm^2, a yield strength of 500 MPa, and an elastic modulus of 210 GPa. For the specimen with the seven-wire strand, a 12.7 mm diameter was selected, with a grade of 1860 MPa. The strand was an uncoated low-relaxation

strand with a nominal cross-sectional area of 97.65 mm^2, and its elastic modulus was 196.5 GPa. The software specified the materials for both the concrete and reinforcement. The solid elements representing the reinforcement utilized the material model with the code CC3DBiLinearSteelVonMises, incorporating the Von Mises Plasticity Model. As for the concrete cube, the material model with the code CC3DNonLinCementitious2 was employed, as indicated in the ATENA Manual. [33]. To determine the parameters of the 3D interface, a thorough investigation is required to select values that describe the mechanical interaction between the bar and concrete. The stiffness coefficients (K_{nn} and K_{tt}) correspond to the stiffness in the normal direction ($K_{\sigma\sigma}$) and the transverse directions (K_{rr} and K_{ss}), as illustrated in Figure 4. Here, (E) and (G) represent the minimal elastic modulus and shear modulus, respectively, of the surrounding material, and (t) is the width of the interface zone. The outermost limit on the tension side of the failure surface curve is denoted by the tensile strength (f_t), while the tangential strength at the initiation of slipping motion is defined as cohesion (c). The inclination of the failure surface upon surpassing the cohesive strength of the interface is determined by the friction coefficient (μ). To ensure positive definiteness even after the interface stiffness was depleted, two additional stiffness values were determined: the minimum normal stiffness, $K_{nn,min}$, and the minimum tangential stiffness, $K_{tt,min}$, specified in the program input. The tension and cohesion softening behaviors proposed by Bruehwiler and Wittman [40], are depicted in Figure 5.

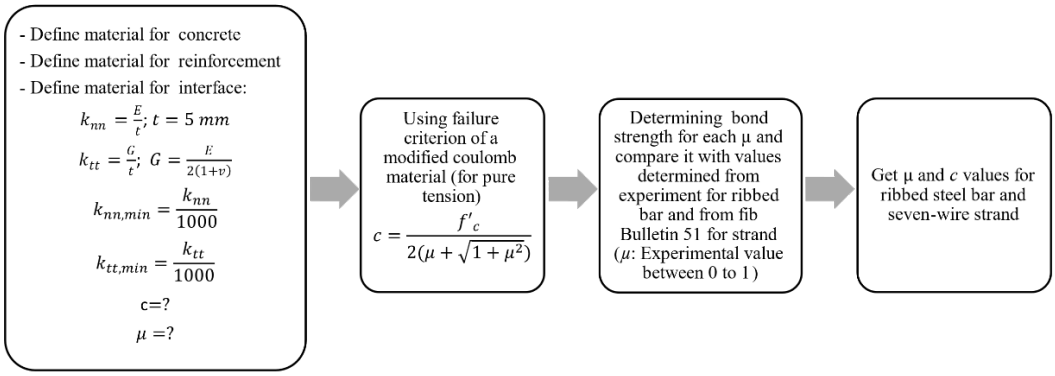

Figure 4: Stage of determining the parameters of the interface between the reinforcement and concrete.

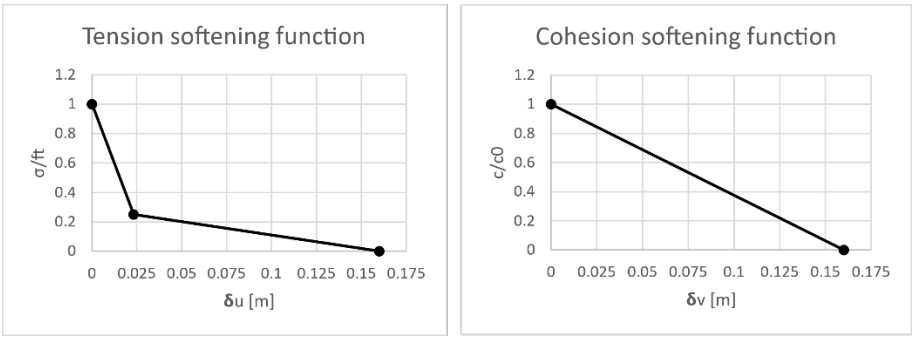

Figure 5: Tension and cohesion softening functions for the interface, with G_f representing the fracture energy of concrete and f_t representing the concrete tensile strength.

To establish the material properties of the 3D interface, various considerations were taken, encompassing the properties of both the concrete and the reinforcement, along with the frictional coefficients (μ and c) governing their interaction. Given the presence of two unknown parameters (μ and c), cohesion could be derived from the known concrete compressive strength and the friction coefficient, and the latter was an experimental parameter ranging from 0 to 1 (refer to Figure 4). Subsequently, the bond strength could be determined for each value of μ. Through a comparison of the obtained bond strength from the

experimental test [3] and Bulletin 51 formula [20], the appropriate value of μ could identified. Noteworthy is the variation in interface characteristics under the same concrete properties, depending on whether a ribbed steel bar or a seven-wire strand is used as reinforcement. This distinction results in different values of μ and c (where c can be calculated based on μ). Thus, c is influenced by both the concrete compressive strength (f'_c) and the friction coefficient (μ), with f'_c being associated with the concrete properties and μ being specific to the type of reinforcement utilized.

Utilizing symmetry, only one-quarter of the specimen section was considered, with enforced boundary lateral restraints on the planes of symmetry. Additionally, vertical support was provided for the top surface of the concrete cube. Various mesh sizes were assessed, including maximum dimensions of 5 mm, 4 mm, and 3 mm. The ATENA 3D software, designed for brick-type meshing only for macro-elements with six boundary surfaces, led to the utilization of tetrahedral FE meshing within the solid element of the steel bar due to its irregular shapes. Tetrahedral FE meshing was applied within the adjacent concrete macro-element containing the bar, while the rest of the concrete body was divided into two macro-elements with six surfaces, modeled using brick finite elements (refer to Figure 6). The concrete zone was assumed to be approximately double the size of the bar. By using tetrahedral FE meshing within the bar and the adjacent concrete macro-element, the bar shared joint locations with the concrete surface. The analysis employed the Standard Newton-Raphson iteration method with displacement load, using an increment of 0.01 mm until specimen failure, with the load applied at the top surface of the reinforcement.

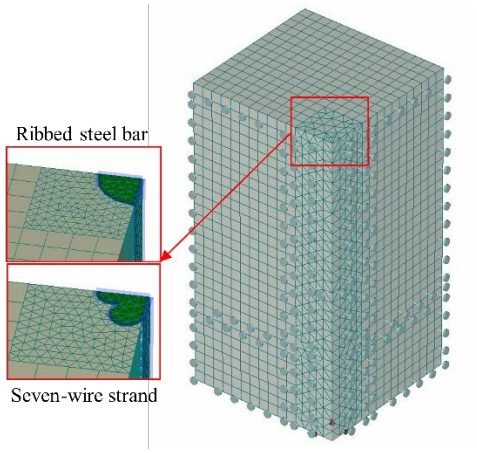

Figure 6: FE model of the pull-out test.

3. Results

3.1. Validation of FE Model

The analysis indicated a consistently small mean relative difference, below 1%, among 5 mm, 4 mm, and 3 mm mesh sizes, suggesting that a 3 mm mesh size was adequate and suitable for the model. Hence, based on this observation and following the approach of Tsiotsias et al. [29], a maximum mesh size of 3 mm was selected. The bond strength for each μ value is illustrated in Figure 7 for both ribbed steel bar and seven-wire strand. The bond strengths from experimental data [3] and the fib Bulletin 51 formula [20] are already established for both types of reinforcement. By determining the appropriate μ value for each type of reinforcement, namely ribbed steel bars and seven-wire strands, the corresponding c value could be identified. The presented values for μ and c in concrete with a compressive strength of 41.65 MPa are (μ = 0.4, c = 14.1 MPa) for the ribbed steel bar, and (μ = 1, c = 8.63 MPa) for the seven-wire strand. Consequently, all parameters of the 3D interface between the reinforcement and concrete are now known.

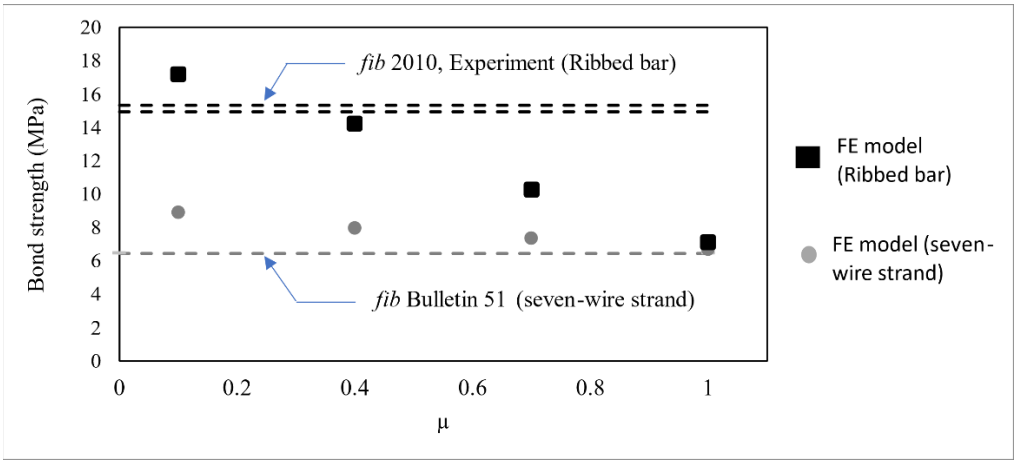

Figure 7: Bond strength obtained numerically for each μ and c values.

3.2. Influence of Steel Diameter on the Bond Strength

In order to examine the impact of reinforcement diameter on bond strength in LWC, the FE model was developed using various reinforcement diameters. Ribbed steel bars with diameters of 8, 10, 12.7, 15.2, and 17.8 mm were employed. For the seven-wire strand, diameters of 12.7, 15.2, and 17.8 mm were utilized. It is evident that the diameter of the reinforcement had an influence on the bond strength, observing a decrease in bond strength as the reinforcement diameter increases (see Figure 8 (a)) as observed by numerous researchers [8–10,36,37,41]. The bond strength (τ_{max}), as demonstrated in Equation 4, is indirectly determined by dividing the developed force carried by the bar (F) by the lateral contact area of the embedment length (l_e). Figure 8 (b) reveals the impact of reinforcement diameter on the pull-out force, indicating that the force increases with larger bar diameters. However, it is important to note that the increase in bar diameter results in a greater contact area, surpassing the effect of force and leading to a reduction in bond strength. Furthermore, Figure 9 showcases the bond stress–slip curve of the FE model, fib MC1990 [42], and fib MC2010 [12] for a seven-wire strand with a diameter of 15.2 mm.

$$\tau_{max} = \frac{F}{P.l_e} \tag{4}$$

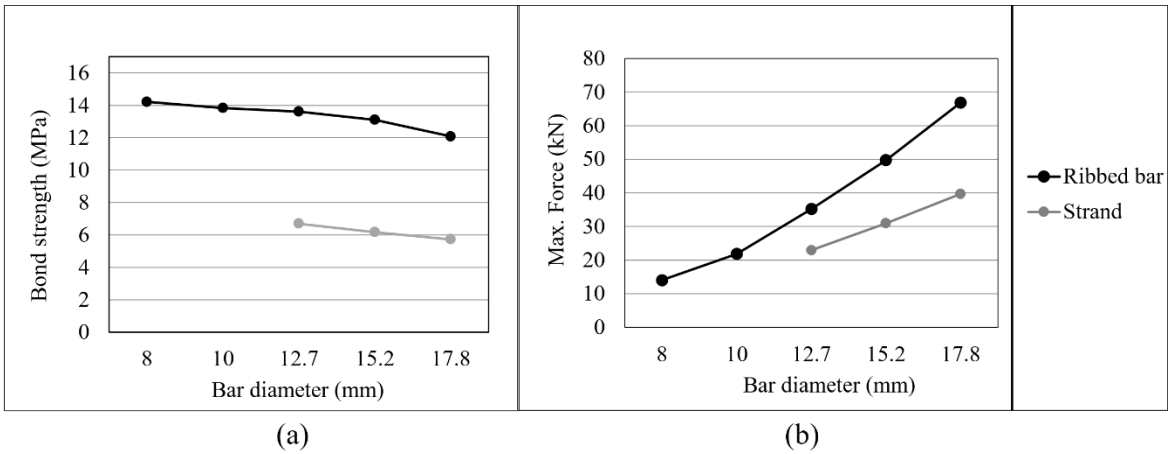

Figure 8: (a) Bond strengths, and (b) Maximum forces of each FE Model.

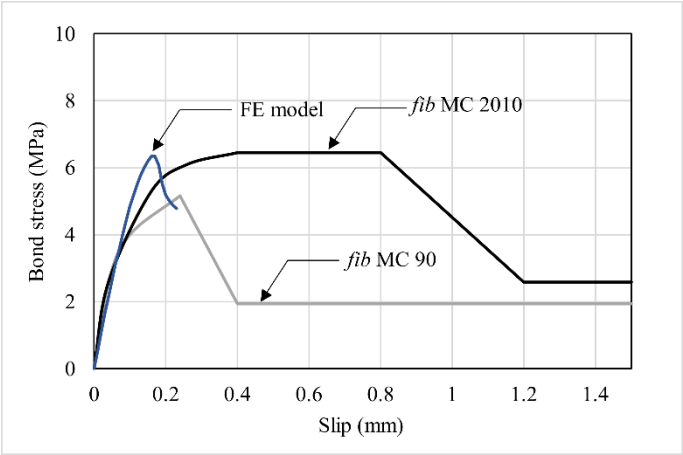

Figure 9: Bond stress–slip relationship of the FE model, fib MC1990, and fib MC2010 for a seven-wire strand with Ø= 15.2 mm.

The numerical results of the bond strength for ribbed steel bars with varying diameters were juxtaposed with the bond strength calculated using different formulae codes, as detailed in Table 1. The formulae, such as fib MC2010 [12] and Harajli et al. [35], considered solely the concrete compressive strength as a significant parameter affecting the bond strength between concrete and steel bars. On the other hand, AS 3600 [36], Orangun et al. [9], and Darwin et al. [37] incorporated the effects of bar diameter, bar cover with the concrete surface, and concrete compressive strength in their formulations. Figure 10 illustrates that the numerical results aligned well with the formulae codes of fib MC2010 [12] and Harajli et al. [35]. Additionally, it was observed that the formulae codes of AS 3600 [33], Orangun et al. [9], and Darwin et al. [37] tended to overestimate the influence of the steel bar diameter.

Table 1: Parametric analysis of maximum bond stress.

Source	Equation (SI Units)
fib MC2010 [12]	$2.5\sqrt{f'_c}$
Harajli et al. [35]	$2.57\sqrt{f'_c}$
AS 3600 [36]	$0.265\left(\frac{c_c}{d_b}+0.5\right)\sqrt{f'_c}$
Orangun et al. [9]	$\frac{18}{\emptyset}+0.776*{f'_c}^{0.5}$
Darwin et al. [37]	$\frac{12.72}{\emptyset}+1.2*{f'_c}^{0.5}$

-

- ; f'_c: Mean value of concrete compressive strength, d_b: Steel diameter, l_b: Embedded length, c_c: Bar cover thickness

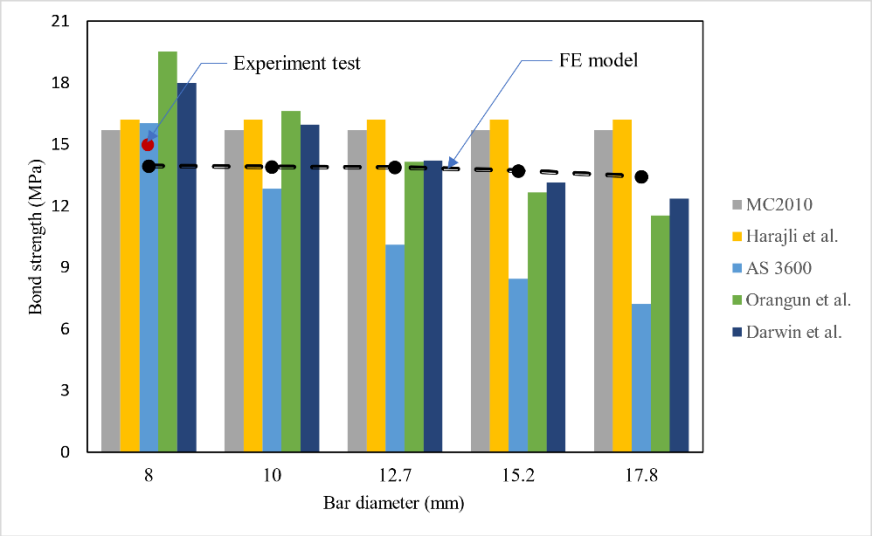

Figure 10: Bond strength of FE Model of ribbed steel bar.

4. Conclusion

Numerical modeling is often preferred when conducting experiments becomes challenging, either due to impracticality, high costs, or time constraints. The investigation aimed to numerically examine the impact of reinforcement diameter, ranging from 8 to 17.8 mm, on bond behavior in the pull-out test. Models for the concrete and reinforcement bars utilized 3D elements, with the interface between the two materials simulated through 3D isoparametric gap elements featuring a pressure-sensitive Mohr-Coulomb frictional interface. The determination of interface parameters involved referencing standardized pull-out test results from previous reports and applying the formula presented in fib Bulletin 51 [20]. The characteristics of the concrete, encompassing tensile strength, elastic modulus, shear modulus, and fracture energy, along with the type of steel bar and its surface condition, served as the basis for determining the main parameters of the interface model. The analysis yielded the following significant discoveries: There exists a divergence of opinions concerning the impact of bar diameter on bond behavior in the pull-out test; however, the FE results indicate a slight reduction in bond strength with an increase in bar diameter. Moreover, the influence on slip values is not notably pronounced for various reinforcement diameters. In addition, the FE findings suggest that the bond strength between the ribbed steel bar and concrete is roughly double that of the seven-wire strand when embedded in concrete. This contrasts with the information provided in fib Bulletin 51 [20], where the bond strength between the seven-wire strand and concrete is reported to be less than 60% of that of the ribbed steel bar.

References

[1] R. Jathar, “Study of Bond Strength of Fibre Reinforced Concrete,” *Int J Res Appl Sci Eng Technol*, vol. 6, no. 4, pp. 2371–2380, Apr. 2018, doi: 10.22214/ijraset.2018.4404.

[2] ACI Committee 440, “Guide Test methods for fiber-reinforced polymers (FRPs) for reinforcing or strengthening concrete structures,” *Farmington Hills, MI: American Concrete Institute*, 2004.

[3] T. Kovács, Z. Gyurkó, L. Jakab, and R. Nemes, “Influence of Unidirectional Cyclic Loading on Bond between Steel Bars Embedded in Lightweight Aggregate Concrete,” *Solids*, vol. 3, no. 3, pp. 397–415, Jul. 2022, doi: 10.3390/solids3030028.

[4] P. R. Shunmuga Vembu and A. K. Ammasi, “A Comprehensive Review on the Factors Affecting Bond Strength in Concrete,” *Buildings*, vol. 13, no. 3, p. 577, Feb. 2023, doi: 10.3390/buildings13030577.

[5] M. Arezoumandi, A. R. Steele, and J. S. Volz, “Evaluation of the Bond Strengths Between Concrete and Reinforcement as a Function of Recycled Concrete Aggregate Replacement Level,” *Structures*, vol. 16, pp. 73–81, 2018, doi: https://doi.org/10.1016/j.istruc.2018.08.012.
[6] N. Majain, A. B. Abd. Rahman, A. Adnan, and R. N. Mohamed, “Bond behaviour of deformed steel bars in steel fibre high-strength self-compacting concrete,” *Constr Build Mater*, vol. 318, p. 125906, 2022, doi: https://doi.org/10.1016/j.conbuildmat.2021.125906.
[7] S. Solyom and G. L. Balázs, “Bond of FRP bars with different surface characteristics,” *Constr Build Mater*, vol. 264, p. 119839, 2020, doi: https://doi.org/10.1016/j.conbuildmat.2020.119839.
[8] Z. P. Bazant and R. Desmorat, “Softening Slip and Size Effect in Bond Fracture,” *ACI Symposium Publication*, vol. 156, doi: 10.14359/1019.
[9] J. O. J. C. O. Orangun and J. E. Breen, “A Reevaulation of Test Data on Development Length and Splices,” *ACI Journal Proceedings*, vol. 74, no. 3, doi: 10.14359/10993.
[10] Y. R. Alharbi, M. Galal, A. A. Abadel, and M. Kohail, “Bond behavior between concrete and steel rebars for stressed elements,” *Ain Shams Engineering Journal*, vol. 12, no. 2, pp. 1231–1239, 2021, doi: https://doi.org/10.1016/j.asej.2020.10.001.
[11] M. Burdziński and M. Niedostatkiewicz, “Experimental-Numerical Analysis of the Effect of Bar Diameter on Bond in Pull-Out Test,” *Buildings*, vol. 12, no. 9, p. 1392, Sep. 2022, doi: 10.3390/buildings12091392.
[12] fib, *fib Model Code for Concrete Structures 2010*. Weinheim, Germany: Wiley-VCH Verlag GmbH & Co. KGaA, 2013. doi: 10.1002/9783433604090.
[13] Z. Huang, B. Engström, and J. Magnusson, “Experimental Investigation of the Bond and Anchorage Behaviour of Deformed Bars in High Strength Concrete (Report 95: 4),” *Chalmers University of Technology: Gothenburg, Sweden*, 1996.
[14] D.-Y. Yoo and H.-O. Shin, “Bond performance of steel rebar embedded in 80–180 MPa ultra-high-strength concrete,” *Cem Concr Compos*, vol. 93, pp. 206–217, Oct. 2018, doi: 10.1016/j.cemconcomp.2018.07.017.
[15] A. J. Tavares, M. P. Barbosa, T. N. Bittencourt, and M. Lorrain, “Bond steel-concrete: simulation analysis of the pull-out tests and APULOT using the program ATENA,” *Revista IBRACON de Estruturas e Materiais*, vol. 7, no. 1, pp. 138–157, Feb. 2014, doi: 10.1590/S1983-41952014000100007.
[16] Z. Alkurdi and T. Kovács, “Analytical and Numerical Modeling of Transfer Length of Seven-wire Strands in Pretensioned Prestressed Concrete Members,” in *18th MIKLÓS IVÁNYI INTERNATIONAL PHD & DLA SYMPOSIUM*, Iványi Péter, Ed., Pécs: Pollack Press, 2022.
[17] International Federation for Structural Concrete, *fib Bulletin 4. Lightweight Aggregate Concrete*. fib, 1999. doi: 10.35789/fib.BULL.0004.
[18] M. A. Abed, Z. Alkurdi, A. Kheshfeh, T. Kovács, and S. Nehme, “Numerical Evaluation of Bond Behavior of Ribbed Steel Bars or Seven-wire Strands Embedded in Lightweight Concrete,” *Periodica Polytechnica Civil Engineering*, vol. 65, no. 2, pp. 385–396, Nov. 2020, doi: 10.3311/PPci.16689.
[19] G. Gulyás, T. Kovács, and R. Nemes, “Bond between strands and high-strength normal-weight and lightweight aggregate concretes,” *Építés - Építészettudomány*, vol. 42, no. 3–4, pp. 261–280, Sep. 2014, doi: 10.1556/EpTud.42.2014.3-4.8.
[20] International Federation for Structural Concrete, *fib Bulletin 51. Structural Concrete Textbook on behaviour, design and performance Second edition Volume 1*. fib, 2009. doi: 10.35789/fib.BULL.0051.
[21] Z. Alkurdi, “Influence of Concrete Compressive Strength on Transfer Length in Pretensioned Concrete Members Using 3D Nonlinear FEM Analysis,” in *6th International Conference On Civil Structural and Transportation Engineering (ICCSTE’21)*, Niagara Falls: AVESTIA, May 2021. doi: 10.11159/iccste21.112.
[22] Z. Alkurdi, “Numerical Study of the Effect of Maximum Aggregate Size on the Ultimate Strength of Pre-tensioned Prestressed Concrete Beam,” *International Journal of Civil Infrastructure*, vol. 5, pp. 70–77, 2022, doi: 10.11159/ijci.2022.010.

[23] Z. Alkurdi, “Evaluation of Pre-tensioned Prestressed Concrete Beam Behavior by Finite Element Analysis Using ATENA 3D,” in *7th International Conference On Civil Structural and Transportation Engineering (ICCSTE’22)*, Niagara Falls: AVESTIA, Jun. 2022. doi: 10.11159/iccste22.192.
[24] W. Don, K. Chong, M. Aitken, A. Tambusay, B. Suryanto, and P. Suprobo, “Influence of link spacing on concrete shear capacity: experimental investigations and finite element studies,” in *IOP Conference Series: Materials Science and Engineering*, IOP Publishing, 2020, p. 012052.
[25] M. A. Abed, Z. Alkurdi, J. Fořt, R. Černý, and S. Solyom, “Bond Behavior of FRP Bars in Lightweight SCC under Direct Pull-Out Conditions: Experimental and Numerical Investigation,” *Materials*, vol. 15, no. 10, p. 3555, May 2022, doi: 10.3390/ma15103555.
[26] J. Červenka and D. Pryl, *ATENA Program Documentation Part 11*. Prague, 2020.
[27] H. Yu and D. Jeong, “Finite Element Bond Modeling for Indented Wires in Pretensioned Concrete Crossties,” in *2016 Joint Rail Conference*, American Society of Mechanical Engineers, Apr. 2016. doi: 10.1115/JRC2016-5782.
[28] A. K. F. Cheung, C. K. Y. Leung, and P. Kabele, “Finite element study on bond behavior of steel bar and HSCC/HSFRCC,” in *Proceedings of the 7th International Conference on Fracture Mechanics of Concrete and Concrete Structures*, 2010, pp. 592–599.
[29] K. Tsiotsias and S. J. Pantazopoulou, “Analytical Investigation on the Effect of Test Setup on Bond Strength,” *CivilEng*, vol. 2, no. 1, pp. 14–34, Jan. 2021, doi: 10.3390/civileng2010002.
[30] A. Vithalkar, “Investigation of interface modelling techniques using finite element analysis with ATENA,” 2019.
[31] M. Smith, *ABAQUS/Standard User’s Manual, Version 6.9*. Providence, RI: Dassault Systèmes Simulia Corp, 2009.
[32] by G. J. D. and J. A. Swanson, *ANSYS engineering analysis system user's manual*. Houston, Pa. : Swanson Analysis Systems, 1985., 1985. [Online]. Available: https://search.library.wisc.edu/catalog/999581007202121
[33] V. Červenka, L. Jendele, and J. Červenka, *ATENA Program Documentation Part 1*. Prague: Červenka Consulting, 2022.
[34] S. De Nardin, F. M. Almeida Filho, J. Oliveira Filho, V. G. Haach, and A. L. H. C. El Debs, “Non-linear Analysis of the Bond Strength Behavior on the Steel-Concrete Interface by Numerical Models and Pull-Out Tests,” in *Structures Congress 2005*, Reston, VA: American Society of Civil Engineers, Apr. 2005, pp. 1–12. doi: 10.1061/40753(171)107.
[35] M. H. Harajli, M. Hout, and W. Jalkh, “Local bond stress-slip behavior of reinforcing bars embedded in plain and fiber concrete,” *Materials Journal*, vol. 92, no. 4, pp. 343–353, 1995.
[36] Standards Australia, *Australian Standard for Concrete Structures*, 2nd ed. North Sydney, NSW: Standards Australia, 1994.
[37] D. Darwin, S. L. McCabe, E. K. Idun, and S. P. Schoenekase, “Development length criteria: bars not confined by transverse reinforcement,” American Concrete Institute, 1992.
[38] A. Windisch, “A modified pull-out test and new evaluation methods for a more real local bond-slip relationship,” *Mater Struct*, vol. 18, no. 3, pp. 181–184, 1985, doi: 10.1007/BF02472967.
[39] T. C. Rilem, “RC 6 Bond test for reinforcement steel. 2. Pull-out test, 1983,” *RILEM recommendations for the testing and use of constructions materials*, pp. 218–220, 1994.
[40] E. Brühwiler and F. H. Wittmann, “The wedge splitting test, a new method of performing stable fracture mechanics tests,” *Eng Fract Mech*, vol. 35, no. 1–3, pp. 117–125, 1990.
[41] D.-Y. Yoo, K.-Y. Kwon, J.-J. Park, and Y.-S. Yoon, “Local bond-slip response of GFRP rebar in ultra-high-performance fiber-reinforced concrete,” *Compos Struct*, vol. 120, pp. 53–64, 2015.
[42] M. C. CEB-FIP, “design code, Comite Euro-International du Beton–Federation Internationale de la Precontrainte.” London, England: Thomas Telford, 1993.